

Biological implications of surf-zone flow complexity

Brian Gaylord¹

Hopkins Marine Station of Stanford University, Pacific Grove, California 93950

Abstract

Wave action imposes potentially large hydrodynamic forces on intertidal plants and animals, and can act as a primary agent of disturbance. It has also been proposed that rapid water accelerations produced by breaking waves might constrain the sizes to which intertidal organisms can grow. However, despite the proven ecological importance of surf-zone flows, few actual measurements of forces imposed on plants or animals by waves in nature have been conducted. In this study, real-time wave forces acting on individuals of the rockweed *Pelvetia compressa* and a sea urchin *Strongylocentrotus purpuratus* are recorded in the field. These measured forces are compared with values predicted from theory using laboratory-determined shape factors (i.e., drag and added mass coefficients) and simultaneous flow measurements conducted adjacent to the deployed samples. Results demonstrate that models predicting large contributions of force due to water's acceleration are likely inaccurate, most probably because such models fail to account for the small spatial scales of surf-zone accelerations. This likely eliminates any capacity for intertidal hydrodynamic accelerational forces to limit size, contrary to previous conjectures. Data also suggest that wave-induced forces predicted from simple fluid dynamic expressions can, but sometimes do not, reflect accurately the forces applied. Together these findings imply that although traditional hydrodynamic theory may indeed provide a valuable tool for predicting forces imposed on immersed surf-zone organisms, such approaches must be used with caution. Finally, the field recordings suggest that sharp, transient forces arising from the impingement of waves directly on non-submerged organisms may in general impose the most severe loadings experienced by intertidal plants and animals, a possibility that to date has received little attention. The precise consequences of such brief forces depend on the level of flexibility or rigidity of an organism's construction.

In intertidal regions of rocky shores, forces imposed by breaking waves may act as one of the dominant mechanisms determining species presence or abundance, plant and animal diversity, and community structure (Lewis 1964; 1968; Dayton 1971; Connell 1978; Paine and Levin 1981; Sousa 1984, 1985; Ricketts et al. 1985). However, despite their importance, wave exposure and the magnitudes of imposed hydrodynamic forces have proven difficult to estimate. Most studies that have attempted to evaluate consequences of breaking waves for intertidal organisms have relied on standard fluid-dynamic theory coupled with idealized flow scenarios that may or may not accurately describe effects of the complex and rapidly evolving water motions of the surf zone (e.g., Koehl 1977; 1984; 1986; Denny et al. 1985; Denny 1987; 1995; Carrington 1990; Denny and Gaines 1990; Dudgeon and Johnson 1992; Bell and Denny 1994; Gaylord et al. 1994; Denny and Gaylord 1996; Blanchette 1997). Thus the validity of models designed to predict the severity or

biological ramifications of forces imposed on intertidal plants and animals has remained an open question.

One unknown in particular has been the precise role played by hydrodynamic forces arising from water acceleration. It has been suggested that in intertidal zones of rocky coasts, hydrodynamic accelerational forces might have the potential to constrain the sizes to which organisms can grow. As originally noted by Denny et al. (1985), hydrodynamic accelerational forces scale with volume while organism strength typically varies in proportion to area (either cross-sectional or attachment area). Because volume generally increases faster than area with increases in size, magnitudes of applied force would be expected to exceed an organism's ability to withstand those forces at some critical maximum size. This basic argument, first applied to stationary intertidal invertebrates by Denny et al. (1985), was also extended by Gaylord et al. (1994) to flexible seaweeds that change shape with growth and reconfigure in flow. Denny and Gaylord (1996) further examined related issues in the context of morphological variation in sea urchins. Each of these studies suggested that hydrodynamic accelerational forces, acting in concert with velocity-dependent forces such as lift or drag, might possess a capacity to limit size or shape in a wide variety of intertidal plants and animals.

Note, however, that due to limited data these preliminary studies were forced to make a number of important first-order simplifications. Specifically, it was assumed that:

1) Large accelerations occur commonly under breaking waves on rocky shores.

2) Surf-zone velocities and accelerations of substantial magnitude can occur simultaneously and along similar lines of action (i.e., velocities and accelerations are not consistently negatively correlated, either temporally or directionally).

¹ Present address: Dept. Ecology, Evolution, and Marine Biology, University of California, Santa Barbara, CA 93106 gaylord@lifesci.ucsb.edu, (805) 893-7397, (805) 893-3777 fax.

Acknowledgments

I am grateful to M. W. Denny for substantive discussions and field and technical assistance. E. C. Bell and B. Hale gave thoughtful feedback on several important points, D. Stokes assisted in the field, J. Lee helped with electronics, S. Thompson provided temporary lab space, and J. Watanabe and C. Baxter shared their ecological expertise. S. Monismith and J. Koseff advised on turbulence issues, S. Mclean and L. Washburn answered a pernicious spectral analysis question, and two anonymous reviewers supplied careful readings and apt suggestions. This study was funded by NSF grant OCE-9313891 to M. W. Denny.

3) Intertidal organisms of a wide variety of shapes are capable of experiencing large hydrodynamic accelerational forces (i.e., accelerational force shape factors, termed added mass coefficients, are not negligibly small).

4) The strong nonuniformity of flows produced under breaking waves does not alter their ability to impose substantial hydrodynamic accelerational loads.

Some evidence has been available for evaluating the appropriateness of these assumptions. For example, initial support for points (1) and (3) was provided by the field and laboratory experiments of Denny (1985), Denny et al. (1985), and Gaylord et al. (1994), which suggested that large accelerations indeed occur in the surf zone and that added mass coefficients of intertidal organisms can be surprisingly large. However, the limited number of measurements conducted in these studies made generalization difficult. More recently, Gaylord (1999) explored explicitly issues (1) and (2) by making high-frequency recordings of velocities and accelerations at multiple intertidal sites along a rocky shore. Results confirmed the ubiquitous presence of rapid accelerations, and showed that they often occur in conjunction with large velocities directed along identical flow axes.

Unfortunately, to date essentially no data have been available for evaluating the validity of assumption (4). The present study attempts to address this gap, while also exploring point (3) more rigorously. This task is undertaken together with a more general examination of the overall ability of traditional hydrodynamic theory to model forces imposed by complex intertidal flows. The following approach is employed.

First, drag parameters (coefficients and exponents of drag) and added mass coefficients of a variety of species are measured in the laboratory. These data verify and extend earlier estimates determined under different flow conditions, and yield clues as to the sensitivity of force parameters to alternative types of fluid motion (issues related to assumption [3] above). Second, real-time field recordings of forces acting on two representative organisms (one flexible, one rigid) are conducted. Water velocities and accelerations are measured adjacent to the samples, and these recordings are combined with laboratory-determined drag and added mass coefficients to make theoretical predictions of force for comparison to measured values (addressing assumption [4] above). Third, spatial scales of velocity and acceleration are examined to evaluate their roles in modulating magnitudes of applied force. Finally, the field measurements are used to explore in a preliminary but quantitative fashion the importance of waves impinging directly on non-submerged plants and animals characterized by differing degrees of compliance.

Materials and methods

Species—Two primary test organisms, one flexible and one rigid, are used in this study. The first of these, the common rockweed *P. compressa* (Fig. 1a) is an extensively branched, perennial brown alga of the Order Fucales which often forms dense beds in mid-intertidal regions of rocky shores exposed to intermediate levels of wave action (Abbott and Hollenberg 1976). Like the majority of intertidal sea-

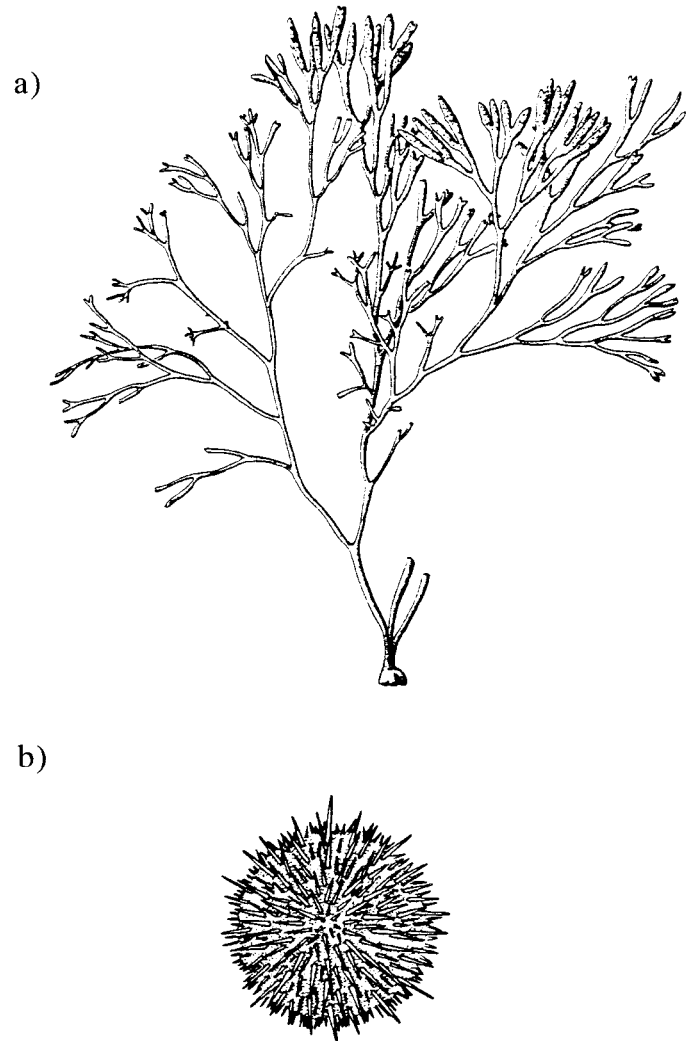


Fig. 1. Primary species used in this study. (a) *P. compressa*. (b) *S. purpuratus*. The organisms are drawn approximately to scale; the diameter of the urchin is about 5 cm.

weeds, this macroalga lays prostrate when emersed at low tide but reorients with flow when exposed to waves. The second focus organism is the purple sea urchin, *S. purpuratus* (Fig. 1b), a spiny echinoderm typically less than 10 cm in diameter that inhabits subtidal to mid-intertidal regions along much of the west coast of North America (Morris et al. 1980). It possesses a calcareous test and therefore deflects little when subjected to hydrodynamic forces. A reduced set of measurements was also conducted on additional species of macroalgae, a limpet, and nonbiological spheres (Table 1).

Flow forces—Studies modeling hydrodynamic forces on sessile marine plants and animals have typically employed simple expressions that are most applicable to rather idealized flow situations (i.e., unidirectional, uniform flow where unsteadiness, if present, doesn't appreciably alter fluid trajectories). These basic equations are outlined below; later

Table 1. Hydrodynamic shape factors in accelerating flow. I_f is the "flatness index," (area^{3/2})/volume, and n is the number of individuals tested, or in the case of *Pelvetia*, the number of experimental runs. SD is the standard deviation. Peak Reynolds numbers for all laboratory experiments ranged from 10^5 to 5×10^5 .

Species and individual	S_d	SD	γ	SD	C_d	SD	I_f	n
Smooth sphere, measured	0.64	0.03	2.0	—	0.40	0.17	—	10
theory	0.47	—	2.0	—	0.5	—	—	—
Rough sphere*	0.62	0.04	2.0	—	1.19	0.37	—	10
Rigid invertebrates								
<i>Lottia gigantea</i> ‡								
a	0.22	0.02	2.0	—	0.37	0.20	—	3
p	0.22	0.01	2.0	—	0.30	0.08	—	3
b	0.48	0.07	2.0	—	0.43	0.19	—	3
<i>Strongylocentrotus purpuratus</i> *	0.67	0.04	2.0	—	1.56	0.17	—	10
Flexible seaweeds								
<i>Calliarthron tuberculosum</i>	0.13	0.04	1.805	0.11	1.63	0.61	33.6	10
<i>Chondracanthus spinosus</i>	0.19	0.07	1.48	0.12	2.16	0.58	34.7	5
<i>Codium fragile</i>	0.19	0.05	1.63	0.35	0.78	0.16	19.7	2
<i>Cryptopleura ruprechtianum</i>	0.13	0.03	1.96	0.19	8.02	1.98	123.9	5
<i>Egregia menziesii</i>	0.12	0.06	2.02	0.21	4.52	1.29	59.5	4
<i>Fucus gardneri</i>	0.12	0.04	1.79	0.18	2.90	0.75	66.8	7
<i>Gelidium purpurascens</i>	0.19	0.06	1.71	0.21	9.35	3.63	55.2	6
<i>Mastocarpus papillatus</i>	0.18	0.04	1.64	0.15	0.58	0.22	5.0	8
<i>Mazzaella flaccida</i>	0.14	0.04	1.52	0.16	4.59	0.87	99.5	9
<i>Pelvetia compressa</i>								
1*	0.21	0.02	1.28	0.06	2.49	0.28	64.9	12
2*	0.23	0.04	1.50	0.10	2.39	0.287	39.0	10
3*	0.30	0.03	1.42	0.07	2.18	0.20	36.1	10
4†	0.35	0.04	1.40	0.09	2.71	0.36	52.0	10
5†	0.26	0.04	1.30	0.10	3.66	0.28	57.5	10
6†	0.25	0.03	1.34	0.08	2.01	0.31	39.8	10
7	0.22	0.02	1.35	0.06	1.57	0.26	47.1	10
8	0.24	0.04	1.42	0.10	3.36	0.29	61.9	10
9	0.20	0.04	1.73	0.20	1.94	0.25	39.5	3
10	0.18	0.02	1.64	0.12	2.28	0.64	47.4	3
11	0.13	0.05	2.00	0.26	5.86	0.48	83.3	5
12	0.14	0.02	1.91	0.09	3.63	0.41	46.4	5
13	0.15	0.04	1.86	0.15	3.89	0.39	43.9	5
average	0.22	0.06	1.55	0.25	1.94	1.15	50.7	13
<i>Pleurophycus gardneri</i>	0.04	0.01	1.50	0.16	1.78	1.06	178.0	2
<i>Prionitis lanceolata</i>	0.37	0.14	1.52	0.07	4.56	0.25	34.8	4

* Samples also tested both in steady flow and in the field.

† Samples also tested in the field.

‡ Anterior upstream (a), posterior upstream (p), or broadside to flow (b).

their utility for estimating intertidal forces is explored in more depth.

Drag pushes objects downstream (Denny 1988; Vogel 1994). It is a function of a fluid's velocity relative to an organism (u_r), and may be expressed as:

$$F_d = \frac{1}{2} \rho A S_d u_r^\gamma, \quad (1)$$

where ρ is the mass density of the fluid and A is the maximum area facing flow. S_d is the shape coefficient of drag and γ is the drag exponent; for rigid organisms that do not change shape as velocities vary, S_d and γ are weak functions only of the nondimensional Reynolds number, $Re = u_r L / \nu$, where L is the length of the organism along the axis of flow and ν is the kinematic viscosity of the

fluid (Vogel 1994). For flexible organisms like seaweeds that passively reconfigure in flow, S_d and γ depend on the magnitude of applied force (and thus the fluid density itself) in addition to Re . Note, however, that because many organisms show a power law velocity-drag relationship in a given fluid medium, both S_d and γ often end up functioning essentially as constants across a considerable range of flow velocities. In general, γ is less than two for flexible plants and animals, but equals two for bluff, rigid organisms. When γ is 2, S_d is equivalent to C_d , the traditional drag coefficient of classical fluid dynamics (Vogel 1984; 1989).

A second category of hydrodynamic force arises from the acceleration of a fluid or organism. Two components of this *hydrodynamic accelerational force* are potentially present. The first of these derives from the pressure gradient respon-

sible for the acceleration of fluid particles, and leads to a virtual buoyancy force:

$$F_{vb} = \rho V \frac{du}{dt}, \quad (2)$$

where V is the volume of the organism and du/dt is the acceleration of the fluid relative to the substratum (Batchelor 1967). F_{vb} is directly analogous to buoyancy (i.e., ρVg , where g is the acceleration due to gravity), but acts along the direction of fluid acceleration rather than just vertically upward. F_{vb} is present only if the fluid itself accelerates.

The second component of hydrodynamic accelerational force results from the relative acceleration between organism and fluid. This added mass force (F_{am}) arises as a consequence of the temporal alteration of momentum required of an evolving flow field diverted around an object (Daniel 1984):

$$F_{am} = C_a \rho V \frac{du_r}{dt}. \quad (3)$$

C_a is the nondimensional added mass coefficient, a function of shape. This force acts in the direction of relative acceleration.

For sessile organisms that do not move substantially with flow (including to a first approximation seaweeds that reorient only through a small fraction of a wave cycle), $u_r = u$, and Eqs. 2 and 3 can be combined into a simple expression for the total hydrodynamic accelerational force (F_a) acting on a stationary organism in an accelerating fluid:

$$F_a = (1 + C_a) \rho V \frac{du}{dt}. \quad (4)$$

Traditionally, the total fore-aft force is then computed as the vector sum of F_d and F_a (Morison et al. 1950). It is this force sum that has been believed to be the proximal source of force-strength scaling that potentially limits size. Note that *lift* (which acts perpendicular to the axis of flow; Vogel 1994) is not addressed in this report but would impose a third component of force when present.

Measurement of drag and added mass coefficients—Accelerating flow: Force parameters were measured using the tow tank shown in Fig. 2. A 200-kg weight and cable/pulley system is used to accelerate a sled with attached sample horizontally through a 3 m long tank of water (40 cm deep, 60 cm wide). The apparatus provides unidirectional relative flow with nearly constant acceleration. Velocities reach 3 m s^{-1} and accelerations 50 m s^{-2} . The sled carries two force transducers: one records the force imposed on a sample attached to it, the second acts as an accelerometer by sensing the inertial force associated with the sled's acceleration. The sample itself, which encompasses less than 5% of the tank cross-section, is held in an inverted posture below a horizontal baseplate. The baseplate has a streamlined leading edge and extends the width of the tank to min-

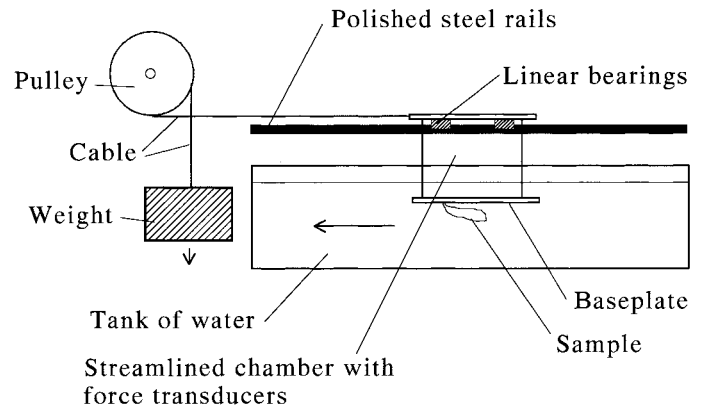


Fig. 2. Tow tank generating unidirectional, relative accelerating flow.

imize vertical and cross-wise flow. Flat planks at the water's surface prevent waves.

The total force sensed by the transducer is assumed to arise from drag and hydrodynamic accelerational forces acting on the sample, plus the inertial force associated with the acceleration of the effective mass of the transducer/sample (m_{eff}):

$$F_{total} = \frac{1}{2} \rho A S_d u_r^\gamma + C_a \rho V \frac{du_r}{dt} + m_{eff} \frac{du_r}{dt}. \quad (5)$$

u_r equals the velocity of the sled, and is calculated by integrating the accelerometer record. Projected areas of the seaweeds (A in Eq. 5) are determined by laying the plants flat, photocopying them, and comparing the weight of their paper silhouettes to that of a piece of paper of known reference area. A similar procedure using photographs is employed for the invertebrates and spheres. Volumes are determined by weighing samples in both air and water and noting that the difference in weight equals $\rho_{wat} Vg$, where $g = 9.81 \text{ m s}^{-2}$ and ρ_{wat} is the water's density. Measurement errors in A and V are estimated to be less than 10 and 2 percent, respectively, and are minor in flexible specimens relative to effects of variable sample reconfiguration among test runs. With A and V known, the parameters S_d , γ , and C_a are found by fitting Eq. 5 (with appropriate substitution of the velocity and acceleration values through time) to recorded hydrodynamic force traces using a least squares curve fitting routine. For rigid samples that do not reorient with flow (i.e., the spheres, limpets, and urchin), γ is set to 2 and the method is used to find simply S_d and C_a . Note that Eq. 5 corrects a typographical error in Denny and Gaylord (1996).

Steady flow: S_d and exponents of drag for three of the seaweed individuals tested in the tow tank were also measured in steady flow using the boat tow device of Utter and Denny (1996) configured with a force transducer. Steady flow drag coefficients of the sea urchin and the rough sphere were determined using the wind tunnel of Denny and Gaylord (1996).

Field measurements of force—Several of the samples tested in the laboratory were also selected for further experimentation in the field. Each sample was attached, one at a time, to a cantilever-style force transducer bolted into an emplacement in the rock within the mid-intertidal mussel zone. The transducer continuously sensed force perpendicular and parallel to the shoreline with a 5 ms time resolution. A drag sphere flow probe (Gaylord 1999) was deployed in a second emplacement 25 cm away to measure water velocities and accelerations. A third emplacement 0.5 m distant contained a pressure transducer (Omega PX176) for sensing the heights of impinging waves. Signals from the three instruments were processed at 1000 Hz. Note that positioning the flow probe adjacent to the force transducer provided a means of comparing actual field-measured hydrodynamic forces to forces predicted from theory (via substitution of the recorded velocities and accelerations and laboratory estimates of S_d , γ , and C_a into Eqs. 1 and 4).

Impingement coefficients—Because the field-tested samples were typically exposed to air just prior to wave arrival, they often experienced impact-type forces (see e.g., Schmidt et al. 1992) due to waves crashing directly against them. To evaluate the importance of these brief but potentially large loads, the maximum applied force during the first 0.5 second of each wave was extracted and compared with the maximum force occurring during the remainder of the wave. These initial-arrival forces are termed impingement forces, F_{imp} , here to distinguish them from true impact loads since not every wave generated a sharp force spike during the half-second impingement interval. The 0.5 s window was chosen based on inspection of the force records which indicated that this interval would insure inclusion of all impact transients detected. Values of F_{imp} were also normalized by the product of area and the dynamic pressure of the flow to provide estimates of impingement coefficients (C_i):

$$C_i = \frac{F_{imp}}{\frac{1}{2}\rho Au^2}, \quad (6)$$

with u set equal to the surf-zone scaling velocity \sqrt{gH} (where H is the inshore wave height), since data (Gaylord 1999) suggest that near-substratum bulk flows under intertidal bores are roughly of this magnitude. C_i is therefore an impingement equivalent to the drag coefficient.

Spatial scales of surf-zone flows—As waves break, large scale water motion associated with a waveform degenerates into turbulent eddies. Although eddies exist across a spectrum of sizes, the largest have dimensions parameterized by the *integral length scale*, λ (Tennekes and Lumley 1972), an index of the largest scale over which velocity fluctuations are typically coherent:

$$\lambda = \int_0^{\infty} R(r) dr, \quad (7)$$

where R is the spatial correlation of velocity fluctuations at a particular position x , given by:

$$R(r) = \frac{\overline{u'(x, t)u'(x + r, t)}}{\overline{u'(x, t)^2}}. \quad (8)$$

In this expression, r is the spatial lag and the overbar indicates temporal averaging. $u'(x, t)$ is the velocity deviation from the mean (U) at position x and time t , while $u'(x + r, t)$ is the simultaneous velocity fluctuation at a distance r from the first measurement. $R(r)$ therefore yields an estimate of the spatial coherence of velocity fluctuations as a function of separation distance, with a value of one indicating that the flows for a given separation r are identical.

In practice, measuring $R(r)$ would require instantaneous flow measurements at multiple spacing intervals (one per each r), a difficult proposition. However, if there is a strong mean flow that advects finer-scale velocity fluctuations past a given location, then a particular temporal lag, τ , can be used as a spatial analogue via the relation $r = U\tau$, an expression termed Taylor's hypothesis. This idealized but fundamental notion of turbulence theory allows the temporal autocorrelation, $R(\tau)$, computed from flow measurements at a single location, to be converted to a spatial correlation (Tennekes and Lumley 1972). The temporal autocorrelation at position x is given by:

$$R(\tau) = \frac{\overline{u'(x, t)u'(x, t + \tau)}}{\overline{u'(x, t)^2}} \quad (9)$$

where τ is the time lag between flow measurements at a single point. The autocorrelation at a time lag of τ therefore equals the spatial correlation at $r = U\tau$ when Taylor's hypothesis holds.

Because Taylor's hypothesis can be grossly violated under breaking waves, only flow records satisfying several criteria were used in the correlation analysis. 2048-point, 1000 Hz segments of velocity were extracted from each wave (filtering out the dominant orbital wave energy) and the mean velocity vector, U , was computed. The 0.5 second impingement interval from each wave was also bypassed in this analysis to avoid artifacts associated with emersion/submersion transitions. Coordinates were then rotated to align with the mean velocity vector of each segment, and the maximum change in the magnitude of U and the maximum perpendicular flow speed were noted. If either quantity or the rms value of u' exceeded $U/5$, then the segment was rejected since these conditions violate the applicability of Taylor's hypothesis (Hinze 1975). If rejected, the process was advanced further through the wave until an acceptable segment was found or the end of the wave was encountered. Multiple segments from each wave were examined. Overall, 937 acceptable segments were found, allowing robust estimation of λ .

In addition to the correlation analysis, a second, point-by-point method was used to evaluate the spatial extent of total velocity (i.e., fluctuations plus any longer term mean), and to determine spatial scales of acceleration since correlation integrals of flow derivatives lose their physical relevance

(they are zero by definition; Tennekes and Lumley 1972). Velocity magnitudes were divided into 1 m s^{-1} bins, and accelerations into 100 m s^{-2} bins. For each of these bins, distributions of the durations of velocity and acceleration were computed, with durations defined as the length of time u or du/dt exceeded continually the bin's lower bound while deviating less than $\pi/4$ radians in direction. Taylor's hypothesis was then invoked to estimate spatial scales of velocity and acceleration for each bin, using \sqrt{gH} as a scaling velocity for the mean flow.

Results

Laboratory measurements of shape factors—Table 1 lists shape coefficients of drag (S_d), drag exponents (γ), and added mass coefficients (C_a) for three categories of samples tested in unidirectional accelerating flow (spheres, rigid invertebrates, and flexible seaweeds).

Two spheres were tested. The first, characterized by a smooth surface, showed both drag and added mass coefficients closely in accordance with other measurements conducted at similar Reynolds number (see e.g., Sarpkaya and Tuter 1974). The exceptional surface texture of the second, rough sphere ($k/D \sim 1/20$, where k is the height of the roughness elements and D the diameter of the sphere) produced a larger added mass coefficient.

Among the rigid invertebrates tested in the tow tank, limpets oriented parallel to flow (either anterior or posterior end forward) showed significantly smaller drag coefficients than when broadside to flow. This difference was about a factor of two, with the S_d 's of the broadside limpets similar to values measured for *S. purpuratus*. The added mass coefficients of the limpets were substantially smaller than that of the nonstreamlined sea urchin. The drag and added mass coefficients of the urchin resemble closely those found previously for *S. purpuratus* at similar Reynolds numbers (Denny and Gaylord 1996).

Like the drag coefficients of the low profile limpets, the S_d 's of the seaweeds were small, a reflection of the tendency of these flexible organisms to passively assume streamlined postures in flow (Koehl 1986; Carrington 1990). Such reconfiguration also produced drag exponents that were less than two (see Vogel 1984; 1989). As found in previous studies (Gaylord et al. 1994), the added mass coefficients of the seaweeds were substantial, typically 4–10 times greater than those of simple shapes such as spheres, and somewhat in excess of the C_a of the spiny urchin.

Table 1 also lists the flatness index ($I_f = A^{3/2}/V$) of each seaweed, a non-dimensional number representing the degree to which a plant grows as a flat sheet. Figure 3a shows S_d 's of seaweed individuals as a function of I_f , suggesting that the shape coefficient of drag declines weakly with increasing flatness index (using an ordinary least squares [OLS] regression with ln-transformed data). In contrast, Figure 3c shows that C_a increases as the flatness index rises (OLS regression with ln-transformed data). The exponent of drag does not appear to depend on I_f (Student's t -test, Fig. 3b). Note that due to the variation in morphology among individuals of a single species, these trends are obscured if only species-averaged S_d or C_a values are used (Table 1).

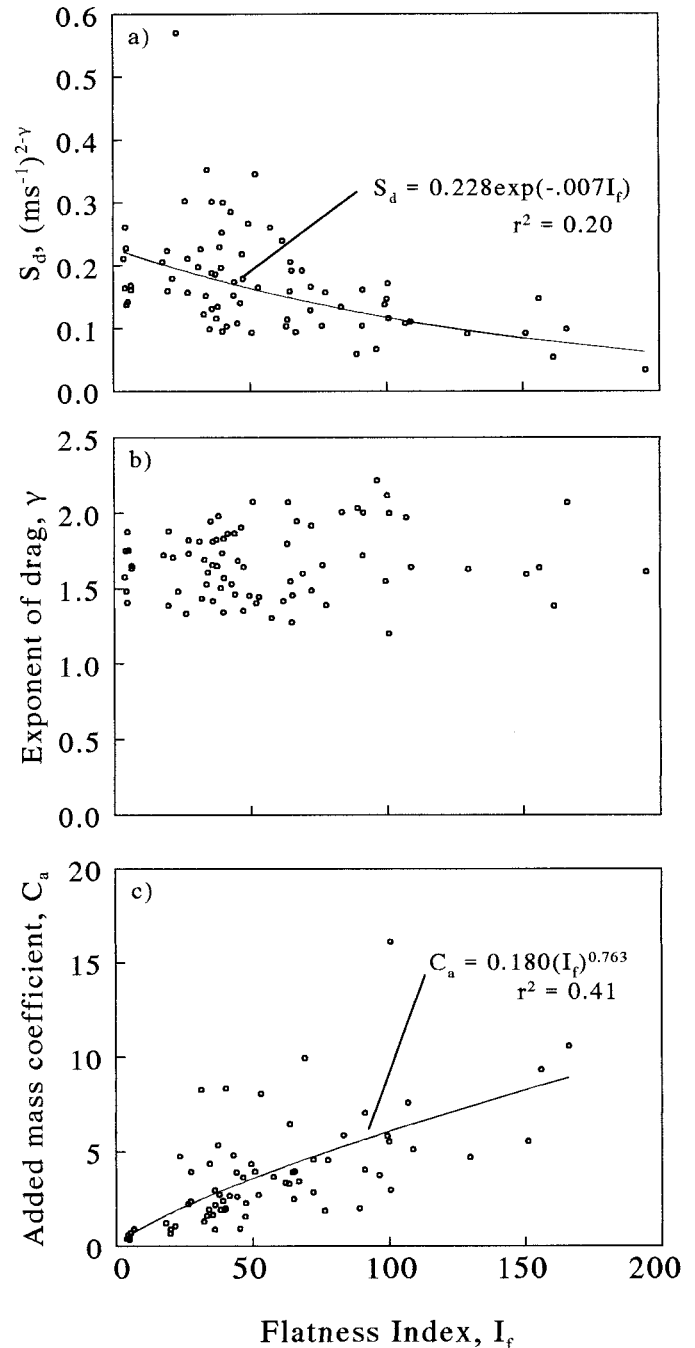


Fig. 3. Force coefficients of multiple species of seaweed as a function of flatness index, $I_f = A^{3/2}/V$, where A is the projected area and V the volume of the alga. (a) Shape coefficients of drag. (b) Exponents of drag. (c) Added mass coefficients.

Hydrodynamic shape factors of field-tested samples—Shape factors of the field-tested samples in accelerating and steady flow are given in Tables 1 and 2, respectively. Drag parameters are similar in the two flow conditions.

Field measurements of force—Wave conditions: Field recordings were conducted on days with rms wave heights at the location of the samples of 0.41–1.26 m (Table 3), typical

Table 2. Morphological and steady flow hydrodynamic parameters of samples tested in the field. Measurements were conducted at a Reynolds number of 10^5 .

Sample	Area (m ²)	Volume (m ³)	Steady flow	
			S_d	γ
<i>Pelvetia compressa</i>				
1	1.7×10^{-2}	3.5×10^{-5}	0.17	1.07
2	1.3×10^{-2}	3.8×10^{-5}	0.18	1.33
3	8.8×10^{-3}	2.3×10^{-5}	0.25	1.26
4	1.8×10^{-2}	4.8×10^{-5}	—	—
5	1.3×10^{-2}	2.7×10^{-5}	—	—
6	9.7×10^{-3}	2.4×10^{-5}	—	—
<i>Strongylocentrotus purpuratus</i>				
Rough sphere (5.33 cm diameter, $k/d = 1/20$)	1.9×10^{-3}	4.1×10^{-5}	0.76	2.0
	2.2×10^{-3}	7.9×10^{-5}	0.74	2.0

of small to moderate winter storms. For 8 of the 11 deployments, waves impinging on the samples were just beginning to break; thus energetic eddy-driven flows associated with the plunging crests of waves had not yet invaded regions near the substratum where the samples were located. Waves that broke in this manner are termed *newly breaking* here (see also Gaylord 1999). During two of the other three field trials, waves broke seaward of the experimental site, propagating to the sample as fully developed bores (identified as *fully breaking* in this report). Insufficient numbers of waves were recorded during the remaining field trial to determine the type of breaking. Note that these breaking classifications reflect the gross level of stochastic motion beneath a wave-form rather than particular phases of a periodic cycle.

The nature of applied forces: Figures 4 and 5 show typical records of hydrodynamic force imposed on four samples through the passage of single waves. Figure 4 presents force records from newly breaking waves acting on a representative *Pelvetia* and the sea urchin. Figure 5 shows forces imposed by fully breaking waves on another *Pelvetia* and the rough sphere. Several trends are visible. Sharp, transient spikes in force occurred at the instant of wave arrival, and the advection of large-scale eddies past the specimens induced substantial temporal variation in force through the re-

mainder of the waves. Also, samples under newly breaking waves generally showed a marked drop in force 1–2 seconds after wave arrival; in contrast, force traces from fully breaking waves did not in general show this decline. Forces under newly breaking waves were often largest during the backwash.

Predicted versus measured forces: Figures 4 and 5 also show the drag predicted from a combination of the laboratory-determined drag parameters and velocity recordings conducted 25 cm away from the samples. Under newly breaking waves, predicted drag exceeded substantially measured forces throughout the central portion of the waves, but matched more closely during the backwash (Fig. 4). In contrast, under fully breaking waves, predicted drag tracked measured forces throughout each wave cycle (Fig. 5). The rationale for plotting only predicted drag, rather than the predicted total force due to the sum of drag and the hydrodynamic accelerational force, is clarified below.

Because flows associated with the central portions of newly breaking waves were of a different character (as evidenced by the marked drop in force, the much greater predicted/measured mismatch, and visual observations of the intensity of turbulence) than those associated with newly breaking backwash or fully breaking waves, the field data were di-

Table 3. Wave conditions during field recording sessions.

Session	Sample	Inshore H_{ms} (m)	Breaker type	Wave period (s)	Tidal height (m)
1	<i>Pelvetia</i> 1	0.78	Newly breaking	13	+1.54
2	<i>Pelvetia</i> 2	0.98	Newly breaking	14	+1.21
3	<i>Strongylocentrotus</i>	0.93	Newly breaking	13	+1.31
4*	<i>Strongylocentrotus</i>	—	—	—	+1.82
5	<i>Pelvetia</i> 3	1.08	Newly breaking	13	+1.40
6	<i>Pelvetia</i> 3	1.26	Newly breaking	12	+1.68
7	<i>Pelvetia</i> 4	0.41	Fully breaking	10	+1.17
8	<i>Pelvetia</i> 5	0.61	Newly breaking	9, 16	+1.23
9	<i>Pelvetia</i> 6	0.69	Newly breaking	16	+1.29
10	Drag sphere	0.55	Newly breaking	17	+0.94
11	Rough sphere	0.52	Fully breaking	8	+0.98

* Insufficient number of recordings on this day to accurately determine wave characteristics.

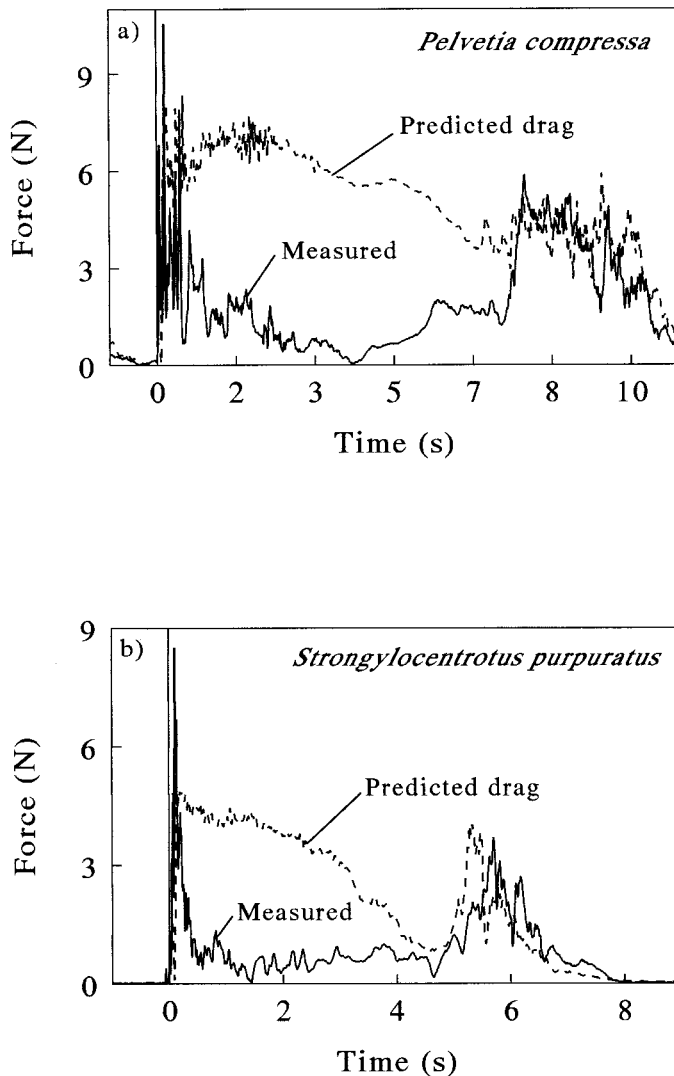


Fig. 4. Representative force traces recorded under newly breaking waves. Note the poor correspondence between predicted drag and measured force throughout the central portion of the wave, followed by an improved match during the wave backwash.

vided into two classes. Force recordings from newly breaking waves, excluding backwash segments, were placed in the first class. Backwash portions were then pooled with measurements from fully breaking waves to create the second class. Once this separation had been accomplished, two sets of comparisons between predicted and measured forces were conducted.

First, maximum measured forces from each wave were compared with maximum predicted total forces (drag plus the hydrodynamic accelerational component) from the same waves. Maxima rather than means were used since extreme forces appear most relevant to organism survival. Under both newly (Fig. 6) and fully breaking flows (Fig. 7), the maximum measured forces were strikingly lower on average than the maximum predicted total forces. This result appears in the graphs as a scatter of points lying mostly below the line passing through the origin with a slope of 1.0. Regres-

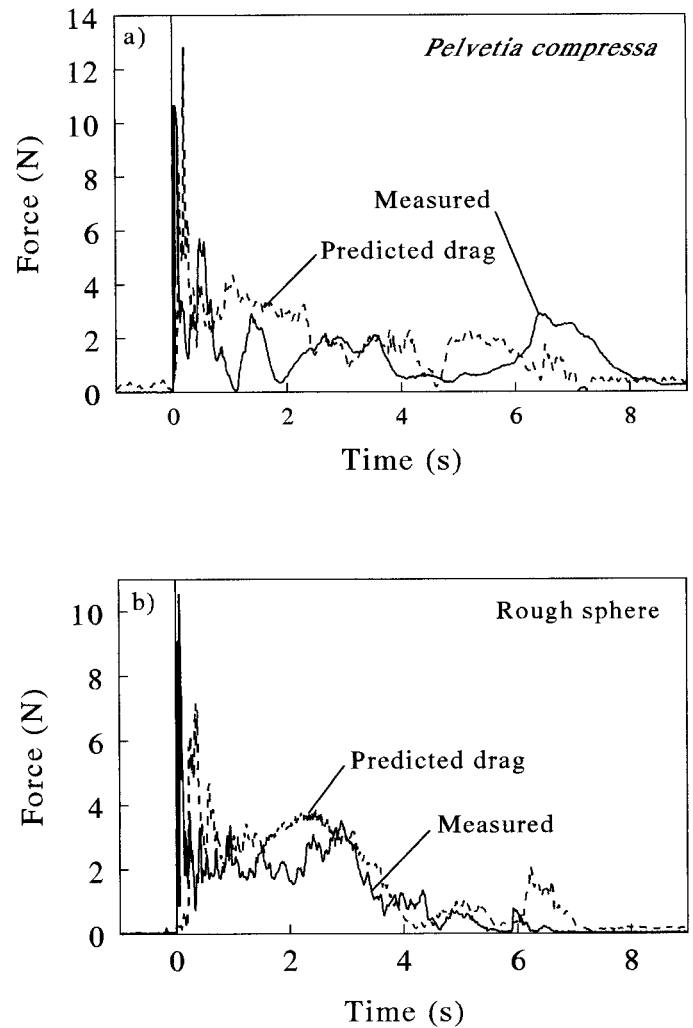


Fig. 5. Representative force traces recorded under fully breaking waves. Note the relatively good correspondence between predicted drag and measured force throughout the entire wave.

sion analyses indicate that slopes of the empirical fits to the data differ significantly ($p < 0.001$) and substantially from 1.0, verifying that measured maximum forces did not match well with predicted total maximum forces (Figs. 6,7).

In the second comparison, the accelerational component of force was subtracted from the predicted total force, leaving only predicted drag, to examine the possibility that the force mismatch was due to overestimation of F_a , (reasons for this expectation are discussed below). This second comparison was conducted only for fully breaking flows since the different character of newly breaking waves suggests the operation of additional processes and a potential for confounding effects of multiple phenomena. Because stochastic water motion in a wave's backwash resembles a fully breaking flow, backwash regions from newly breaking waves were again pooled with the fully breaking data. Figure 8 shows the measured maximum forces relative to the maximum predicted drag under fully breaking flows. Note that although regression statistics indicate that empirical fits again have slopes that differ from 1.0 ($p < 0.01$ in Fig. 8a and $p <$

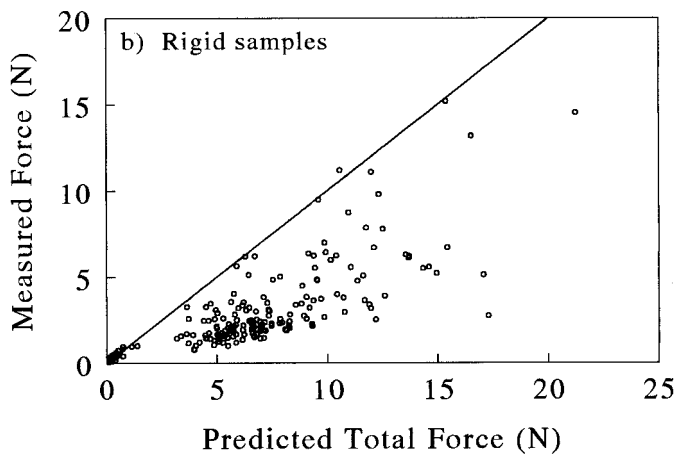
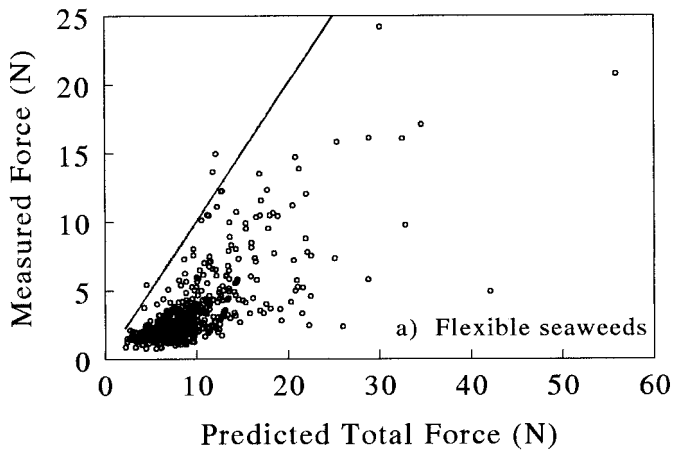


Fig. 6. Measured maximal forces versus predicted maximal total forces from all newly breaking waves, excluding backwash segments.

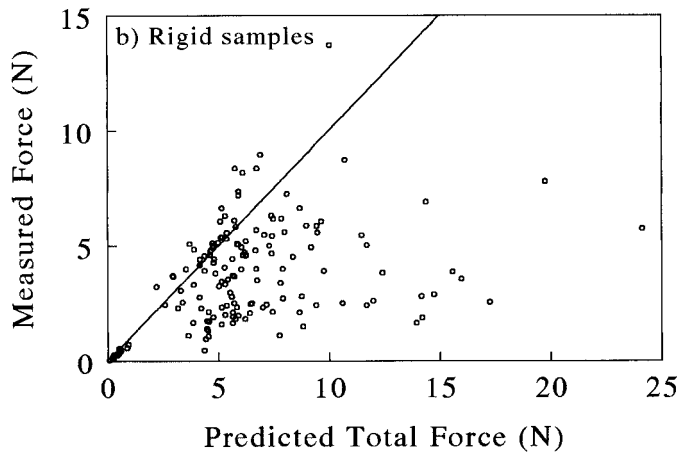
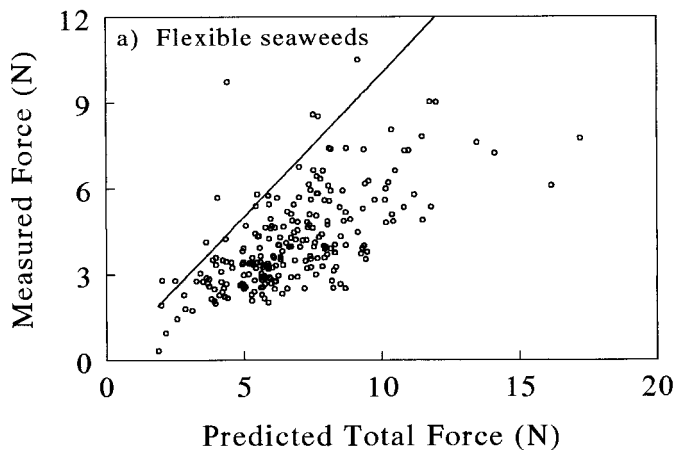


Fig. 7. Measured maximal forces versus predicted maximal total forces from all fully breaking waves and backwash of newly breaking waves.

0.05 in Fig. 8b), the deviations from 1.0 are not large (slopes are 0.86 and 0.80 in Figs 8a and 8b, with 95% confidence intervals of 0.11 and 0.17, respectively). Similarly, the y-intercepts are near zero; the origin actually falls within the 95% confidence bounds in Fig. 8a. These results suggest that the simple drag equation, ignoring accelerational effects entirely, may adequately predict the maximum forces imposed by fully breaking flows.

Impingement forces: The force maxima in Figs 6 to 8 exclude predicted/measured data from the first 0.5 s of each wave since impact effects cannot be modeled by Eqns. 1 or 4. However, the largest forces encountered by samples were often impingement forces. Figure 9 shows the histograms of the ratio of impingement to maximum non-impingement force, for both the flexible seaweeds and the rigid samples under fully breaking conditions. The mean force ratios are 1.8 and 2.5 for the flexible and rigid samples, respectively, indicating that on average impingement forces exceeded subsequent hydrodynamic forces by about a factor of two. However, attention only to the means of these distributions may

be misleading. Among the impingement forces used to calculate the distributions of Fig. 9, only a subset correspond to impact-type transients, suggesting that the large fraction of force ratios near one reflects the sporadic nature of impact events rather than their typical magnitude. The long right hand tail of the histograms in Fig. 9 supports this view, emphasizing that impact loads may be larger than classical hydrodynamic forces by as much as a factor of 4 to 10, depending on organism flexibility.

Note that the rigid samples experienced greater numbers of large F_i/F_d ratios than *Pelvetia* individuals. Further evidence for this trend is provided in Figure 10 which shows the histograms of the ratio of impingement coefficient to drag coefficient for the seaweeds and rigid specimens. These data show that even after normalizing by C_d to account for effects of differential streamlining, rigid samples still exhibit a tendency to experience relatively greater impingement coefficients than the seaweeds. Note that C_d 's of the seaweeds (which are functions of velocity) were calculated from their shape coefficients of drag using the expression $C_d = S_d u^{\gamma-2}$ with velocities approximated by the surf-zone scaling veloc-

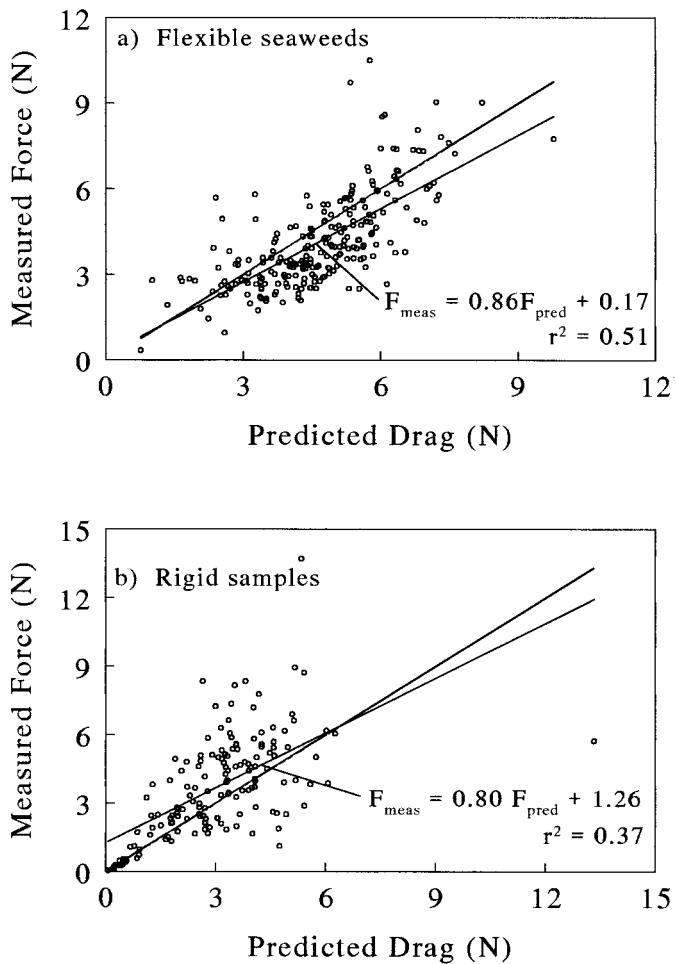


Fig. 8. Measured maximal forces versus predicted maximal drag from all fully breaking waves and backwash of newly breaking waves.

ity \sqrt{gH} . Thus the algal C_d 's used in this comparison are those that characterize the plants at the approximate velocities producing the impingement forces to which they have been subjected.

Spatial scales—The application of Taylor's hypothesis to the fully breaking velocity records yields the average velocity spatial correlation curve shown in Fig. 11a. The corresponding integral scale, λ , is 0.04 m, suggesting that the largest eddies 2 cm above the substratum under breaking waves are about 4 cm across. This length scale is about a fifth as large as those reported by Flick and George (1990) for surf zone flows 20 cm above a smooth sandy beach. It is also about twice as large as the elevation above the bottom of the sensing element of the flow probe, and is therefore consistent with order of magnitude expectations provided by turbulence theory (e.g., Svendsen 1987).

Note that because there is a substantial, more slowly varying mean flow (upon which velocity fluctuations are superimposed), the results shown in Fig. 11a do not imply that velocities of a given magnitude span only a 4 cm region. Rather, the correlation analysis indicates simply that the size

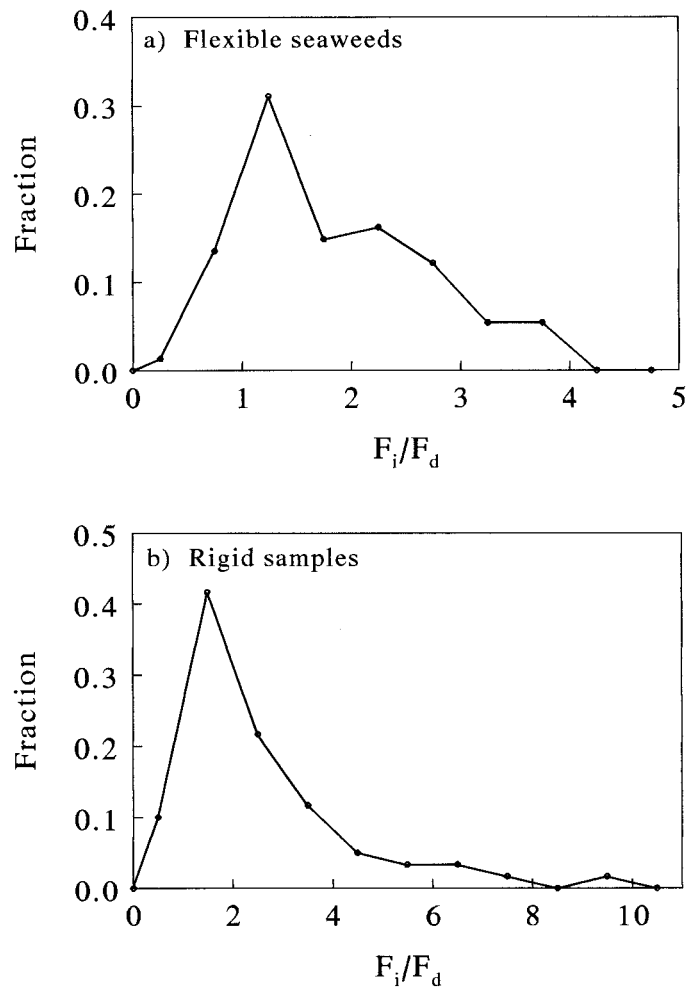


Fig. 9. Histogram of the ratio of impingement force to maximum non-impingement force for all fully breaking waves. Note the difference in x-axis scaling between the two panels.

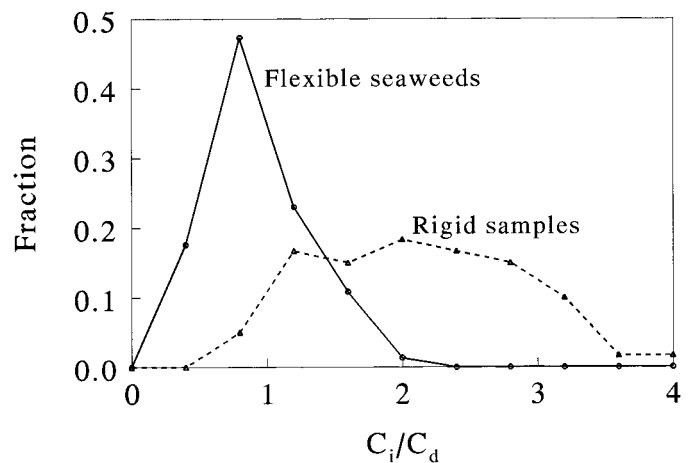


Fig. 10. Histogram of the ratio of impingement coefficient to drag coefficient for all fully breaking waves.

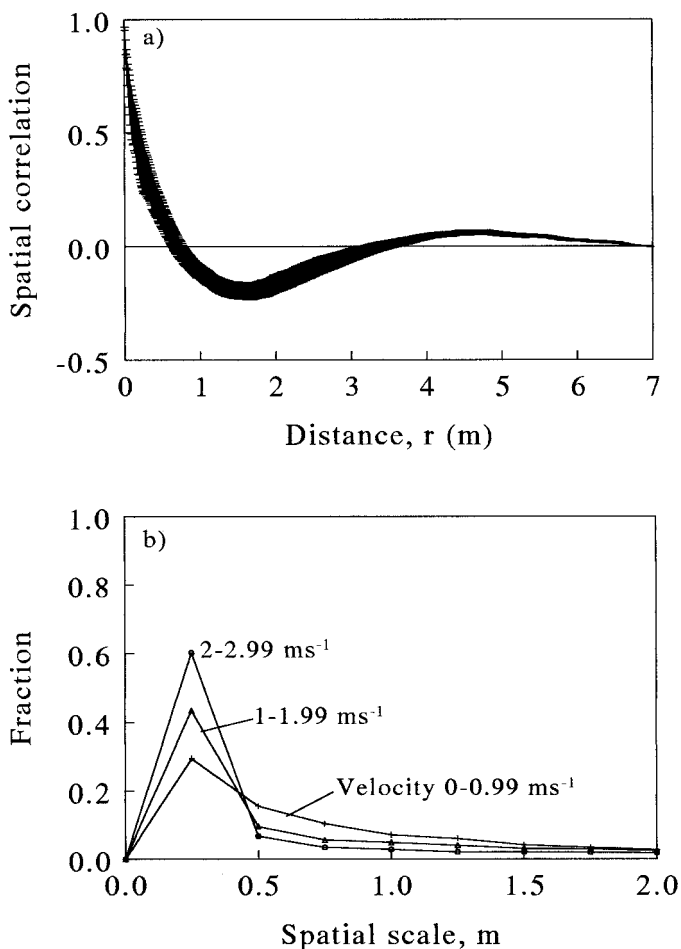


Fig. 11. Spatial scales of surf-zone velocity. (a) Spatial correlation curve. The integral of this function yields an index of the size of the dominant eddies (here approximately 4 cm). The width of the curve indicates the variance at a given spatial lag. (b) Spatial scales of total velocity, accounting for effects of the mean flow.

of the dominant eddies at 2 cm above the substratum are approximately of this size. This point is made explicitly in Fig. 11b via the point-by-point spatial scale analysis. These data indicate that total velocities typically have a spatial extent of approximately 0.2–0.5 m. Note that the distinction between Figs 11a and 11b is that the former computes the spatial scale of the eddies only, while the latter superimposes any longer term mean flow onto the eddies and thus indicates the spatial extent of total velocity.

Results from the spatial analysis of acceleration are given in Fig. 12. These data indicate that spatial scales of acceleration are one and a half orders of magnitude smaller than those of total velocity, and are characterized by dimensions of order 1 cm (note also that because this scale is of the same general size as the flow probe sensor, this may actually be a slight overestimate due to limits on resolution). Implications of this small scale are addressed in the Discussion.

Discussion

Drag parameters and flow conditions—Results from the present study, coupled with steady-flow measurements by

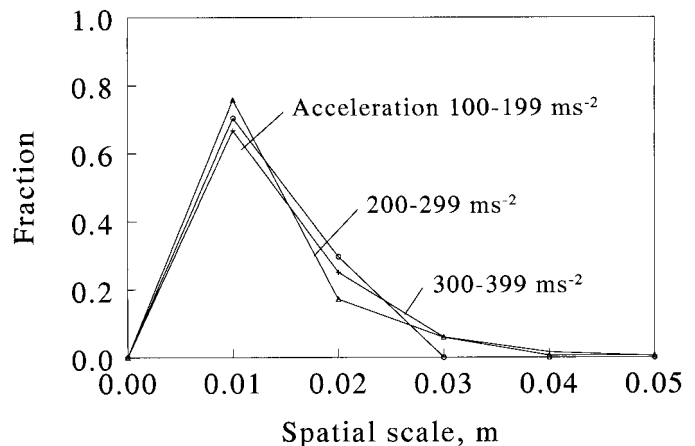


Fig. 12. Spatial scales of surf-zone acceleration.

several researchers (e.g., Denny et al. 1985; Carrington 1990; Dudgeon and Johnson 1992; Johnson and Koehl 1994; Denny 1995; Gaylord and Denny 1997) and experiments in both steady and accelerating flow (Denny and Gaylord 1996; Gaylord et al. 1994), suggest that coefficients and exponents of drag of marine organisms are similar in several types of flow when Reynolds number and fluid density are held constant. For example, Carrington (1990) made extensive drag measurements in steady flow in water on the alga *Mastocarpus papillatus* and presents a master drag curve for 139 individuals of this species where S_d equals 0.16 and γ is 1.63. These numbers are very close to the species-averaged values found for the eight *Mastocarpus* individuals tested in unidirectional accelerating flow at roughly the same peak Re (Table 1). Analogously, Gaylord et al. (1994) found drag coefficients of three other species of intertidal macroalgae, measured in both steady and sinusoidal oscillatory water flow at equivalent peak velocities, to be similar, and tow tank measurements on *Mazzaella flaccida* (previously *Iridaea flaccida*, Hommersand et al. 1993) also yielded drag coefficients resembling closely those recorded in oscillatory flow at similar Re (Gaylord et al. 1994). These findings are probably not surprising; other researchers have demonstrated that the drag coefficients of spheres and cylinders, for example, are similar in steady and oscillatory flow as long as flow excursions between reversals are large (Sarpkaya and Isaacson 1981).

Added mass coefficients and flow conditions: The limited data that exist also suggest that added mass coefficients of marine organisms in oscillatory and unidirectional accelerating flow are comparable at equivalent Re. For example, *M. flaccida* showed a C_a of 4.58 in oscillatory flow (Gaylord et al. 1994) and a value of 4.59 from the tow tank. It also appears that such large C_a 's are common among complexly shaped organisms (Gaylord et al. 1994; Denny and Gaylord 1996; Table 1).

At least two mechanisms may lead to large C_a 's. Gaylord et al. (1994) noted that a flexible sheet of plastic and a flat-bladed alga experienced larger added mass coefficients than more highly clumped species, with values resembling those of hollow perforated spheres. Thus they proposed that sea-

weeds may experience large C_a 's by trapping fluid within a complexly branched frond mass or by rolling up to enclose water inside. The idea was that this could increase the effective volume of a plant, and would appear as a large added mass coefficient when represented in the form of Eq. 4.

While fluid entrapment may indeed play a role in the development of large added mass coefficients of some organisms, measurements of the present study suggest another possibility as well. Figure 3c shows that flatter algae (even those incapable of rolling up in flow) tend to experience larger C_a 's than more foliose plants. This trend is opposite to what one would expect if fluid entrapment were the primary mechanism inducing large added mass coefficients. Instead, it is possible that large C_a 's follow from thinner organisms disturbing a larger volume of fluid relative to their own volume than bulkier individuals. Because added mass effects arise as a consequence of the temporal alteration of fluid's momentum in the vicinity of an object, a fluttering behavior could produce larger relative added mass forces. Until further tests are completed, however, this possibility remains hypothetical.

Newly breaking waves: Why the mismatch?: As is clear from Fig. 4, measured forces under newly breaking waves are predicted only poorly by traditional theories, regardless of whether the accelerational component is included or not. Although a complete explanation of this discrepancy will require further experimental study, several potential mechanisms that could have conceivably contributed to it (the majority of which likely did not) are sketched below.

Several of the most obvious possibilities can be dismissed out of hand. Calibration errors, the use of incorrect shape coefficients, or improper area or volume estimates appear unlikely due to the fact that predicted/measured forces match closely under fully breaking waves and during newly breaking backwash (Figs. 4,5). The force discrepancy also cannot be ascribed to organism flexibility since mismatches occurred for both rigid and reorienting samples (Fig. 4). All of the field-tested organisms (including the rigid sea urchin, which cannot flatten against the substratum) protruded from the substratum distances similar to the probe; thus the mismatch does also not appear to be a consequence of differential positioning within the boundary layer.

Another possibility is that flows at the location of the velocity probe were consistently more rapid than those in the vicinity of the sample. However, when two identical drag sphere shapes were deployed at the site, separated by 25 cm, the forces acting on each were on average the same. The relative magnitudes of measured and predicted forces also did not change when the positions of flow probe and sample organism were swapped.

Laboratory studies have also indicated that drag coefficients of objects can depend strongly on the nature of turbulence within a flow (e.g., Neve and Shansonga 1989; Denny 1994). However, the relevance of such results to the complexly shaped and exceptionally rough samples of the present study is unclear. Many of the turbulence effects noted by Neve and Shansonga (1989), for example, involve the interaction of turbulent eddies with the separation point and wake behind a smooth sphere. For rough or irregularly

shaped organisms, impinging turbulence may play a lesser role in modifying instantaneous patterns of flow. Thus, although consequences of such turbulence effects cannot be discounted, their ability to explain the patterns observed under newly breaking waves remains uncertain.

Therefore although there are many factors that may have contributed to the observed mismatch between predicted and field-measured forces under newly breaking waves, no simple, stand-alone explanation is obvious. There is some hint that fine-scale details of flow or drag coefficient variation, perhaps mediated by gradients in turbulence intensity, may play a role in modifying fluid-imposed forces. Further experimentation, however, is clearly required before this issue can be resolved. Despite the incongruence of predicted and observed forces under newly breaking flows, however, it is perhaps worth emphasizing that the data also indicate that traditional hydrodynamic theory can under many conditions predict accurately the forces imposed on intertidal organisms (Fig. 8). This appears to be the case under fully breaking waves and under newly breaking waves during the backwash (Figs. 4,5). Note that Koehl (1977) also found rough agreement between predicted and measured forces during her field experiments with sea anemones.

The absence of large hydrodynamic accelerational forces: Although previous studies suggested a robust potential for intertidal plants and animals to experience large hydrodynamic accelerational forces, they left untested the question as to whether the complexity of intertidal flows alters their ability to impose such loads. Evidence in this report suggests that this issue is of critical importance. Figures 6–8 show that maximum measured forces are predicted best by considering drag alone, completely ignoring acceleration. Although these comparisons include only peak forces from each wave, there is also no sign of sporadically imposed, large F_a forces. Over the course of all field trials, 82 waves produced accelerations in excess of 100 m s^{-2} (Table 4). This acceleration magnitude would have been expected to impose forces of 7.41–16.76 N, not counting drag, depending on the size and C_a of the sample. In comparison, only 29 waves produced total maximum forces, including drag, in excess of these predicted F_a quantities. Furthermore, in no case did actual maximum forces exceed maximum predicted total forces by more than 6 N, while the overall maximum predicted F_a (52.59 N), was over 28 N in excess of the largest total force measured.

These data, together with previous work, suggest that although (1) rapid accelerations occur under breaking waves (Denny 1985; Denny et al. 1985; Gaylord 1999), and even though (2) they occur in association with velocities of substantial magnitude (Gaylord 1999), and while (3) added mass coefficients are nontrivial in a number of different flow regimes (Gaylord et al. 1994; Denny and Gaylord 1996; Table 1), large hydrodynamic accelerational forces are not commonly imposed on surf-zone organisms. The most likely reason for this discrepancy revolves around the small spatial scales of intertidal accelerations. Because their length scales are only of order 1 cm, accelerations likely vary strongly across the dimensions of most macroscopic plants and animals, interacting with them as nonuniform flow fields (mak-

Table 4. Occurrence of large accelerations in the field. F_a is the hydrodynamic accelerational force predicted for the given sample based on a particular acceleration magnitude, and n is the number of waves during the sample recording session that produced accelerations in excess of that magnitude. Note that the F_a values include no contribution from drag, while the maximum measured-force values do.

Sample	Acceleration magnitude								Maximum measured total flow force (N)
	100 ms ⁻²		200 ms ⁻²		300 ms ⁻²		400 ms ⁻²		
	F_a (N)	n	F_a (N)	n	F_a (N)	n	F_a (N)	n	
<i>Pelvetia</i> 1	12.46	2	—	—	—	—	—	—	10.45
<i>Pelvetia</i> 2	13.15	25	26.29	6	39.44	1	52.59	1	24.20
<i>Pelvetia</i> 3	7.41	29	14.83	6	22.23	1	—	—	15.82
<i>Pelvetia</i> 4	—	—	—	—	—	—	—	—	10.50
<i>Pelvetia</i> 5	12.93	11	25.87	1	—	—	—	—	5.98
<i>Pelvetia</i> 6	7.41	2	—	—	—	—	—	—	5.43
<i>Stongylocentrotus</i>	10.88	12	—	—	—	—	—	—	15.20
Rough sphere	16.76	1	—	—	—	—	—	—	13.72

ing a direct application of Eqs. 2–4 invalid), and preventing the imposition of coherent accelerational forces. In contrast, the larger spatial scales of velocity (Fig. 11) insure that drag can occur unabated. Note that although tiny inhabitants of rocky shores can in theory be encompassed by a 1-cm wide accelerational flow field, such denizens are so diminutive that the volume-dependent hydrodynamic accelerational force becomes insignificant relative to lift or drag (which vary in proportion to area and therefore become dominant at small scales).

Implications for size constraints: The apparent inability of surf-zone accelerations to impose large loads also likely prevents them from constraining size in intertidal organisms. Nevertheless, the original size-related patterns noted by Denny et al. (1985) do appear to exist. Wave-swept organisms rarely exceed 2–3 m in their greatest dimension, and are often smaller in exposed sites than in protected habitats. Intertidal organisms are also strikingly smaller than plants and animals living elsewhere (e.g., subtidal kelps growing outside the breaker zone, or for that matter, terrestrial trees) which may reach tens of meters in length. This raises the question as to whether there could be other physical factors that might have the potential to impose size constraints on intertidal organisms. At least one possibility exists for flexible organisms.

Recently, Gaylord and Denny (1997) and Denny et al. (1997; 1998) have suggested that inertial forces may become important for flexible but attached organisms that move in response to flow and get jerked to a halt when they reach the limits of their ranges of motion. Because inertial forces scale with mass, and since mass and volume are proportional, a scenario again arises where applied forces may become increasingly large relative to organism strength as a plant or animal gets larger (Carrington [1990] has noted a possible analogous situation resulting from plants' allometric growth). Whether the scaling associated with organism momentum might actually impart constraints in nature, however, awaits further study. Note that such a mechanism would apply only to flexible organisms since rigid creatures do not build sufficient inertia for this effect to become important. Denny (in press) discusses in more detail current views on potential surf-zone size limits.

Wave impingement and flexibility: While hydrodynamic accelerational forces have been perhaps incorrectly implicated in intertidal flow disturbance, Fig. 9 suggests that wave impingement effects on organisms have been just as inappropriately overlooked. Historically, although coastal engineers have devoted much effort to the study of impact forces (e.g., Miller et al. 1974; Blackmore and Hewson 1984; Cooker and Peregrine 1990), intertidal biologists have typically discounted the importance of wave impact for two reasons. First, it has been believed that flows with high fractions of entrained air are less likely to produce large pressure transients, and breaking waves on rocky shores provide excellent examples of white water. Second, the only previous measurements conducted on rocky shores that had sufficient temporal resolution to detect impact transients did not show any (Denny 1985). While it now appears that the precise site used by Denny (1985) may have been rather unique in this regard, the possibility that wave impact may in fact be quite common on wave-swept shores has become evident only recently. With their emerging potential importance in mind, we now explore briefly how impingement forces might arise and their relationship to organism compliance.

As noted in the Materials and Methods, impingement coefficients are computed by normalizing F_i by a term containing the dynamic pressure, the pressure that would be applied if the flow were smoothly brought to a halt (Denny 1988; Vogel 1994). This normalization is not done purely for convenience, but because there is a relationship between dynamic pressure and the physics involved in producing impingement loads. To understand this link, we examine a form of Euler's equation (see, e.g., Fox and McDonald 1985), essentially a per-volume, frictionless fluid-dynamic equivalent to Newton's 2nd law:

$$-\frac{dp}{dx} = \rho \left(\frac{\partial u}{\partial t} + u \frac{\partial u}{\partial x} \right), \quad (10)$$

where the term in brackets equals the total derivative du/dt , expanded here to emphasize that the rate of change of u depends on both space and time. dp/dx is the pressure gradient along the axis of flow.

If the flow is steady, the first term in brackets becomes

zero. Under these conditions, Eq. 10 can be integrated with respect to x to give the well-known Bernoulli's equation for steady flow along a horizontal streamline (Vogel 1994):

$$p + \frac{1}{2}\rho u^2 = \text{constant}, \quad (11)$$

This expression indicates that if fluid particles moving along a fluid trajectory in steady flow come to a stop, p concomitantly increases by an amount equal to the dynamic pressure. It is in comparing this situation to what happens during the initial impact of waves against an organism where the distinction between impingement loads and standard hydrodynamic forces becomes apparent.

When an organism is immersed in a steady flow, there is to a first approximation only a spatial gradient in velocity (i.e., $\partial u/\partial x$ is finite, but $\partial u/\partial t$ is zero), with C_d providing an index of the fraction of the organism's frontal area over which dynamic pressure must act to impose the same drag as that actually experienced. In contrast, when a moving fluid first impacts a non-submerged plant or animal, the flow field has to rapidly evolve to establish a new set of fluid trajectories that pass around the organism. Thus velocities are forced to change in time as well as space (in this way the impingement phenomenon is analogous to an added mass effect without the volumetric scaling), and the $\partial u/\partial t$ term in Eqn. 10 becomes large. This in turn requires a greater pressure gradient. When indexed in terms of the dynamic pressure, this increased pressure appears as a larger C_i coefficient, one that can exceed substantially typical C_d values.

Note also that this overall impingement process may be modulated by organism compliance. Because flexible organisms move with the flow, they provide more time for an impacting fluid to evolve a new set of trajectories. This may allow the same eventual flow pattern to be achieved with lower temporal rates of change in velocity and thereby lower applied pressures and forces. Furthermore, as Koehl (1982; 1984; 1986) has noted, because flexible plants and animals often lay prostrate until extended by flow, brief flow events may not have time to both reposition and stretch an organism during the short duration of a force impulse. In contrast, rigid invertebrates such as urchins have shorter response times and therefore may be more vulnerable to impingement effects.

Conclusions

Several points emerge from this study. First, comparison of drag parameters and added mass coefficients among several types of flow suggest that hydrodynamic shape factors of organisms can be relatively insensitive to gross, large scale characteristics of relative water motion, if the Reynolds number and fluid medium remain the same. The laboratory accelerating flow measurements also confirm the existence of large added mass coefficients in many intertidal plants and animals. Second, the field measurements demonstrate that the elementary drag equation can, but does not always, describe effectively the fluid-dynamic forces imposed by breaking waves. This issue requires additional experimentation to explore the factors that may lead to occasional or

chronic overestimation of force under waves that are just beginning to break. Third, the measurements of this study indicate that substantial hydrodynamic accelerational forces do not act commonly either on rigid invertebrates or flexible macroalgae in the intertidal zone. This result arises not from a lack of large fluid accelerations, a canceling out of effects of velocity and acceleration, or an intrinsic inability of organisms to experience hydrodynamic accelerational loads, but instead most likely follows from the exceptionally fine-scale spatial variation of the accelerations produced by breaking waves. This feature probably eliminates the ability of hydrodynamic accelerational forces to constrain sizes of intertidal plants and animals. Finally, the impingement of waves on nonsubmerged organisms appears to be a general mechanism that may impose the largest forces typically encountered by surf-zone creatures, particularly for rigid organisms that respond quickly to brief loads. This highly stochastic phenomenon merits additional attention, particularly since it cannot be modeled using traditional hydrodynamic equations designed to predict forces on immersed plants and animals.

References

- ABBOTT, I. A., AND G. J. HOLLENBERG. 1976. Marine Algae of California. Stanford Univ. Press.
- BACHELOR, G. K. 1967. An Introduction to Fluid Dynamics. Cambridge Univ. Press.
- BELL, E. C., AND M. W. DENNY. 1994. Quantifying wave exposure: A simple device for recording maximum velocity and results of its use at several field sites. *J. Exp. Mar. Biol. Ecol.* **181**: 9–29.
- BLACKMORE, P. A., AND P. J. HEWSON. 1984. Experiments on full-scale wave impact pressures. *Coastal Eng.* **8**: 331–346.
- BLANCHETTE, C. A. 1997. Size and survival of intertidal plants in response to wave action: A case study with *Fucus garneri*. *Ecology* **78**: 1563–1578.
- CARRINGTON, E. 1990. Drag and dislodgment of an intertidal macroalga: Consequences of morphological variation in *Mastocarpus papillatus* Kutzing. *J. Exp. Mar. Biol. Ecol.* **139**: 185–200.
- CONNELL, J. H. 1978. Diversity in tropical rain forests and coral reefs. *Science* **199**: 1302–1310.
- COOKER, M. J., AND D. H. PEREGRINE. 1990. A model for breaking wave impact pressures. *Proc. 22nd Coastal Eng. Conf.*, p. 1473–1486.
- DANIEL, T. L. 1984. Unsteady aspects of aquatic locomotion. *Am. Zool.* **24**: 121–134.
- DAYTON, P. K. 1971. Competition, disturbance, and community organization: The provision and subsequent utilization of space in a rocky intertidal community. *Ecol. Monogr.* **41**: 351–389.
- DENNY, M. W. 1985. Wave forces on intertidal organisms: A case study. *Limnol. Oceanogr.* **30**: 1171–1187.
- . 1987. Life in the maelstrom: The biomechanics of wave-swept rocky shores. *Trends Ecol. Evol.* **2**: 61–66.
- . 1988. Biology and the mechanics of the wave-swept environment. Princeton Univ. Press.
- . 1994. Extreme drag forces and the survival of wind- and water-swept organisms. *J. Exp. Biol.* **194**: 97–115.
- . 1995. Predicting physical disturbance: Mechanistic approaches to the study of survivorship on wave-swept shores. *Ecol. Monogr.* **65**: 371–418.
- . In press. Mechanical limits to size in wave-swept organisms? *J. Exp. Biol.*

- , DANIEL, T. L., AND M. A. R. KOEHL. 1985. Mechanical limits to size in wave-swept organisms. *Ecol. Monogr.* **55**: 69–102.
- , AND S. D. GAINES. 1990. On the prediction of maximal intertidal wave forces. *Limnol. Oceanogr.* **35**: 1–15.
- , AND B. GAYLORD. 1996. Why the urchin lost its spines: Hydrodynamic forces and survivorship in three echinoids. *J. Exp. Biol.* **199**: 717–729.
- , GAYLORD, B., AND E. A. COWEN. 1997. Flow and flexibility II. The roles of size and shape in determining wave forces on the bull kelp *Nereocystis luetkeana*. *J. Exp. Biol.* **200**: 3165–3183.
- , ———, B. HELMUTH, B., AND T. L. DANIEL. 1998. The menace of momentum: Dynamic forces on flexible organisms. *Limnol. Oceanogr.* **43**: 955–968.
- DUDGEON, S. R., AND A. S. JOHNSON. 1992. Thick vs. thin: Thallus morphology and tissue mechanics influence differential drag and dislodgement of two co-dominant seaweeds. *J. Exp. Mar. Biol. Ecol.* **165**: 23–43.
- FLICK, R. E., AND R. A. GEORGE. 1990. Turbulence scales in the surf and swash. *Proc. 22nd Coastal Eng. Conf.* pp. 557–569.
- FOX, R. W., AND A. T. McDONALD. 1985. *Introduction to Fluid Mechanics*. John Wiley and Sons.
- GAYLORD, B. 1999. Detailing agents of physical disturbance: Wave-induced velocities and accelerations on a rocky shore. *J. Exp. Mar. Biol. Ecol.* **239**: 85–124.
- , C. A. BLANCHETTE, AND M. W. DENNY. 1994. Mechanical consequences of size in wave-swept algae. *Ecol. Monogr.* **64**: 287–313.
- , AND M. W. DENNY. 1997. Flow and flexibility I. Effects of size, shape, and stiffness in determining wave forces on the stipitate kelps *Eisenia arborea* and *Pterygophora californica*. *J. Exp. Biol.* **200**: 3141–3164.
- HINZE, J. O. 1975. *Turbulence*. McGraw-Hill.
- HOMMERSAND, M. H., M. D. GUIRY, S. FREDERICQ, AND G. L. LEISTER. 1993. New perspectives in the taxonomy of the Gigartinales (Gigartinales, Rhodophyta). *Hydrobiologia* **260/261**: 105–120.
- JOHNSON, A. S., AND M. A. R. KOEHL. 1994. Maintenance of dynamic strain similarity and environmental stress factor in different flow habitats: Thallus allometry and material properties of a giant kelp. *J. Exp. Biol.* **195**: 381–410.
- KOEHL, M. A. R. 1977. Effects of sea anemones on the flow forces they encounter. *J. Exp. Biol.* **69**: 87–105.
- . 1982. The interaction of moving water and sessile organisms. *Sci. Am.* **247**: 124–134.
- . 1984. How do benthic organisms withstand moving water? *Amer. Zool.* **24**: 57–70.
- . 1986. Seaweeds in moving water: Form and mechanical function, p. 603–634. *In* T. J. Givnish, [ed.] *On the Economy of Plant Form and Function*. Cambridge Univ. Press.
- LEWIS, J. R. 1964. *Ecology of rocky shores*. English Univ. Press.
- . 1968. Water movements and their role in rocky shore ecology. *Sarsia* **34**: 13–36.
- MILLER, R. L., S. LEVERETTE, AND J. O'SULLIVAN. 1974. Field measurements of impact pressures in surf. *Proc. 14th Coastal Eng. Conf.*, pp. 1761–1777.
- MORISON, J. R., M. P. O'BRIEN, AND J. W. JOHNSON. 1950. The forces exerted by surface waves on piles. *Petroleum Trans. AIME* **189**: 149–157.
- MORRIS, R. H., D. P. ABBOTT, AND E. C. HADERLIE. 1980. *Intertidal invertebrates of California*. Stanford Univ. Press.
- NEVE, R. S., AND T. SHANSONGA. 1989. The effects of turbulence characteristics on sphere drag. *Int. J. Heat Fluid Flow* **10**: 318–321.
- PAINE, R. T., AND S. A. LEVIN. 1981. Intertidal landscapes: Disturbance and the dynamics of pattern. *Ecol. Monogr.* **51**: 145–178.
- RICKETTS, E. F., J. CALVIN, J. W. HEDGPETH, AND D. W. PHILLIPS. 1985. *Between Pacific tides*, 5th ed.. Stanford Univ. Press.
- SARPKAYA, T., AND M. ISAACSON. 1981. *Mechanics of wave forces on offshore structures*. Van Nostrand Reinhold.
- , AND O. TUTER. 1974. Forces on cylinders and spheres in a sinusoidally oscillating fluid. Naval Postgraduate School Tech. Rep. NPS-59SL74091. Naval Postgraduate School.
- SCHMIDT, R., H. OUMERACI, AND H. PARTENSKY. 1992. Impact loads induced by plunging breakers on vertical structures. *Proc. 23rd Coastal Eng. Conf.*, p. 1545–1559.
- SOUSA, W. P. 1984. The role of disturbance in natural communities. *Annu. Rev. Ecol. Syst.* **15**: 353–391.
- SOUSA, W. P. 1985. Disturbance and patch dynamics on rocky intertidal shores, p. 101–124. *In* S. T. A. Pickett and P. S. White, [eds.], *The Ecology of Natural Disturbance and Patch Dynamics*. Academic Press.
- SVENDSEN, I. A. 1987. Analysis of surf zone turbulence. *J. Geophys. Res.* **92**: 5115–5124.
- TENNEKES, H., AND J. L. LUMLEY. 1972. *A first course in turbulence*. MIT Press.
- UTTER, B. D., AND M. W. DENNY. 1996. Wave-induced forces on the giant kelp *Macrocystis pyrifera* (Agardh): Field test of computational model. *J. Exp. Biol.* **199**: 2645–2654.
- VOGEL, S. 1984. Drag and flexibility in sessile organisms. *Am. Zool.* **24**: 34–44.
- . 1989. Drag and reconfiguration of broad leaves in high winds. *J. Exp. Bot.* **40**: 941–948.
- . 1994. *Life in Moving Fluids*, 2nd ed. Princeton Univ. Press.

Received: 12 April 1999

Accepted: 7 September 1999

Amended: 24 September 1999